THE JOURNAL OF BIOLOGICAL CHEMISTRY VOL. 289, NO. 32, pp. 21877–21887, August 8, 2014
© 2014 by The American Society for Biochemistry and Molecular Biology, Inc. Published in the U.S.A.

The Calcium-induced Conformation and Glycosylation of Scavenger-rich Cysteine Repeat (SRCR) Domains of Glycoprotein 340 Influence the High Affinity Interaction with Antigen I/II Homologs*[S]

Received for publication, March 17, 2014, and in revised form, June 10, 2014 Published, JBC Papers in Press, June 12, 2014, DOI 10.1074/jbc.M114.565507

Sangeetha Purushotham and Champion Deivanayagam[1]

From the Department of Vision Sciences/Center for Structural Biology, University of Alabama at Birmingham, Birmingham, Alabama 35294-4400

Background: AgI/II homolog interaction with GP340 is crucial for bacterial attachment to tooth surface.
Results: Tandem SRCR domains efficiently adhere/aggregate bacteria. Calcium-induced conformational switch and *O*-linked carbohydrates of SRCRs are necessary for the interaction with AgI/II homologs.
Conclusion: High affinity interactions are dictated by calcium and carbohydrates.
Significance: Oral streptococci adhere to specific calcium-induced conformation of immobilized SRCRs and to its carbohydrates.

Oral streptococci adhere to tooth-immobilized glycoprotein 340 (GP340) via the surface protein antigen I/II (AgI/II) and its homologs as the first step in pathogenesis. Studying this interaction using recombinant proteins, we observed that calcium increases the conformational stability of the scavenger-rich cysteine repeat (SRCRs) domains of GP340. Our results also show that AgI/II adheres specifically with nanomolar affinity to the calcium-induced SRCR conformation in an immobilized state and not in solution. This interaction is significantly dependent on the *O*-linked carbohydrates present on the SRCRs. This study also establishes that a single SRCR domain of GP340 contains the two surfaces to which the apical and C-terminal regions of AgI/II non-competitively adhere. Compared with the single SRCR domain, the three tandem SRCR domains displayed a collective/cooperative increase in their bacterial adherence and aggregation. The previously described SRCRP2 peptide that was shown to aggregate several oral streptococci displayed limited aggregation and also non-specific adherence compared to SRCR domains. Finally, we show distinct species-specific adherence/aggregation between *Streptococcus mutans* AgI/II and *Streptococcus gordonii* SspB in their interaction with the SRCRs. This study concludes that identification of the metal ion and carbohydrate adherence motifs on both SRCRs and AgI/II homologs could lead to the development of anti-adhesive inhibitors that could deter the adherence of pathogenic oral streptococci and thereby prevent the onset of infections.

The attachment of bacteria to human tissue and other surfaces within the oral cavity is thought to be an essential first step in pathogenesis, and microbes utilize surface proteins (pili and fimbrae) to effectively adhere to a variety of molecules and surfaces. The oral cavity is home to a number of microbes, including oral streptococci, where the mutans streptococci (*Streptococcus mutans* and *Streptococcus sobrinus*) are the known etiological agents in dental caries, and the viridians streptococci (*Streptococcus gordonii* and *Streptococcus sanguis*) are considered to be the commensal flora. Among the surface proteins on oral streptococci, antigen I/II (AgI/II)[2] homologs (also known as P1, PAc, SpaP, and SR) in *S. mutans* (1–3), SspA and SspB in *S. gordonii* (4–7), and Pas in *Streptococcus intermedius,* etc. (8, 9) are the most well studied. These AgI/II homologs adhere to tooth-immobilized salivary agglutinin (SAG) secreted by the parotid gland (10, 11). Typically, AgI/II homologs carry a signal sequence at the N terminus, followed by the alanine-rich (A), variable (V), and proline-rich (P) regions, followed by the C-terminal region and the membrane spanning domain that anchors to the bacterial cell wall (Fig. 1). In earlier studies, we identified two SAG adherence regions on AgI/II (12, 13), one at the apex of the molecule (A_3VP_1) and the other at the C terminus (C_{123}), specifically the C_1 and C_2 domains that adopt the DEv-IgG fold, a variant of the classical IgG-fold (14). More importantly we determined that these two regions adhere to SAG in a non-competitive manner, indicating the presence of two different surfaces on SAG, pointing toward bacterial heterogeneity (multivalency) in adherence (13). So far, these interactions were studied with extracted and purified SAG (some groups address purified SAG as GP340) (15, 16) from single or multiple donors and in some cases with saliva itself (17, 18). The presence of allelic variability among donors and their associated post-translational modifications, an established standard has been lacking to quantify these interactions. This study now establishes the first benchmark using recombinantly expressed subdomains of SAG that are involved in microbial adherence.

* This work was supported, in whole or in part, by National Institutes of Health Grant R01DE017737.
[S] This article contains supplemental Figs. S1–S6 and Tables S1 and S2.
[1] To whom correspondence should be addressed: Dept. of Vision Sciences/Center for Structural Biology, 1025 18th St. South, CBSE 100, University of Alabama at Birmingham, Birmingham, AL 35294-4400. Tel.: 205-934-6026; E-mail: champy@uab.edu.

[2] The abbreviations used are: AgI/II, antigen I/II; GP340, glycoprotein 340; SRCR, scavenger receptor cysteine-rich domain; SAG, salivary agglutinin; RU, resonance unit; SPR, surface plasmon resonance; ZP, zona pellucida; FAM, fluorescein amidite.

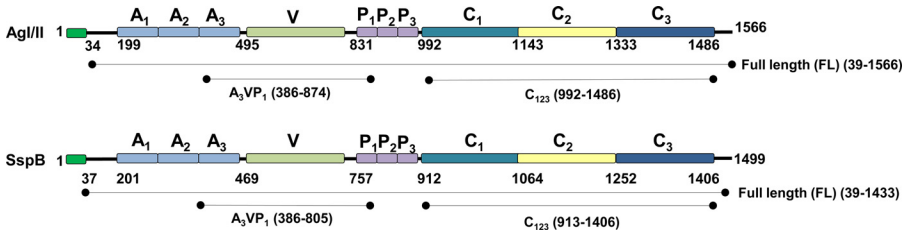

FIGURE 1. **Schematic representation of primary sequence of *S. mutans* UA159 AgI/II and *S. gordonii* DL1 SspB, including the extents of the recombinant fragments shown here.**

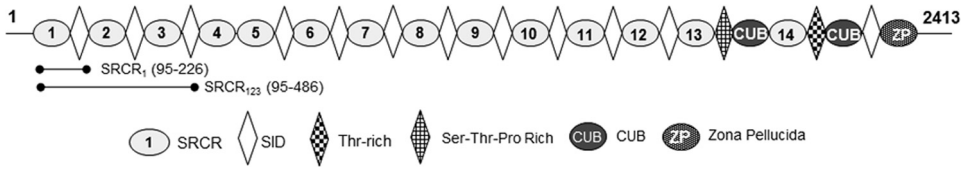

FIGURE 2. **Schematic representation of primary sequence of GP340's 13 tandem SRCR domains, the CUB, and ZP are shown here.** The figure also includes the extents of the recombinantly expressed *i*SRCR$_1$ and *i*SRCR$_{123}$ (33).

SAG is a large glycoprotein complex that contains glycoprotein 340 (GP340), sIgA, and an unknown 80-kDa protein (10, 19). Among these, the major component GP340 is known to aggregate several species of bacteria, including mutans, viridans streptococci, and *Helicobacter pylori* (18, 20), and is thereby considered an innate immune response factor. GP340 is a 340-kDa protein that contains 14 SRCR domains, two C1r/C1s Uegf Bmp1 (CUB) domains, and one zona pellucida (ZP) domain (Fig. 2). The 13 SRCR domains are present in tandem at the N terminus, followed by an intriguingly nested 14th SRCR domain between two CUB domains, with a ZP domain at the C terminus. The SRCR domains are interspersed with regions termed SID, an acronym for the SRCR interspersed domains. Except between the 4th and the 5th SRCR domain, all other tandem repeats contain the SID domain (11). These SRCR domains belong to an ancient class of proteins and are present in protozoan parasites like *Cryptosporidium*, *Toxoplasma, Plasmodium*, and in the algae *Chlamydomonas* (21, 22). They also appear in the entire animal kingdom, beginning with sponges, and are highly conserved, where a single SRCR domain usually contains 100–110 amino acids (23). GP340 SRCR domains were recently shown to aid in transcytosis of HIV into vaginal epithelial cells (24, 25). This highlights the role of the GP340 SRCR domains in infection, where it serves as a portal of entry into the host for both bacteria and viruses that result in various human diseases (26–29).

In a systematic study conducted with various oral streptococci, Loimaranta *et al.* (30) classified bacterial recognition properties of GP340 into three different groups as follows: group I strains were both aggregated by and adhered to GP340; group II preferentially adhered, and group III preferentially aggregated. Using a peptide-based approach, Bikker *et al.* (17, 31) identified a consensus peptide SRCRP2 (QGRVEVLYRGSWGTVC) derived from the 14 SRCR domains of GP340, which aggregated several species of bacteria, and also inhibited the adherence of AgI/II to SAG (32). In a subsequent study using alanine scanning, the most important residues involved in aggregation were deduced to reside within the "VEVL*XXXX*W" motif (31). In these studies, the SID domains that are predicted to host the glycosylation sites were classified into two different groups, namely SID20 and SID22 based on sequence homology, and neither one displayed aggregation nor adherence to bacteria (17, 31).

In this study, we have reported the adherence characteristics and the multicomponent adherence mechanisms adopted by *S. mutans* AgI/II and *S. gordonii* SspB with the recombinantly expressed SRCR domains. We also have presented comparative results on the adherence and aggregation properties of the SRCRP2 peptide and recombinantly expressed SRCRs. The results emanating from this study would foster the development of inhibitors to AgI/II homologs on oral streptococci.

EXPERIMENTAL PROCEDURES

Expression and Purification of Proteins—*i*SRCR$_1$ and *i*SRCR$_{123}$ were expressed and purified as described recently by Purushotham *et al.* (33), and AgI/II fragments used in this study were prepared as described previously (12, 13). SspB constructs Full length (FL^{SspB}) (39-1433), $A_3VP_1^{SspB}$ (386-805), and C_{123}^{SspB} (913-1406), were cloned into the pET23d vector (Novagen) using primers listed in supplemental Table S1, restriction enzymes NcoI, NotI, BamHI, and XhoI, and the template plasmid containing the *SspB* gene (Fig. 1). Similar to methods described earlier for *S. mutans* AgI/II (12, 13), the SspB fragments were purified over three columns, HisPrep nickel affinity, Mono Q, and Superdex 200 10/300 GL gel filtration. The purified fragments FL^{SspB} (154.8 kDa), $A_3VP_1^{SspB}$ (47.7 kDa), and C_{123}^{SspB} (56.2 kDa) were qualitatively assessed to be >95% pure from SDS-polyacrylamide gels (supplemental Fig. S1).

Surface Plasmon Resonance—Real time binding analyses of the SRCR domains with AgI/II fragments were carried out using the BIAcore 2000 system. The CM5 chip was labeled with ligands *i*SRCR$_1$ or *i*SRCR$_{123}$ or SAG as described previously (34, 35), using the amine coupling kit (GE Healthcare). The control and experimental surfaces were blocked using 1 M ethanolamine. Various concentrations of analytes (0.125 to 2.5 μM) of *S. mutans* AgI/II or *S. gordonii* SspB fragments (supplemental Table S2) were injected over the prepared chip surfaces, and dissociations were measured for 8–10 min at a flow rate of 20 μl/min of binding buffer (20 mM HEPES, pH 7.4, 150 mM

NaCl, 2.5 mM $CaCl_2$) at 25 °C. Self-adhesion of *i*$SRCR_1$ or *i*$SRCR_{123}$ (2 μM) was also determined in a similar manner as described above. Between experiments, the regeneration of the chip surface was accomplished using solutions as shown in supplemental Table S2. Finally, to determine the effect of calcium, SPR analysis was carried out by dialyzing the analytes and ligands in binding buffer devoid of $CaCl_2$.

On-chip enzymatic deglycosylation of the *i*$SRCR_1$ and *i*$SRCR_{123}$ was carried out to remove *N*- and *O*-linked carbohydrates. Briefly, after immobilization of *i*$SRCR_1$ and *i*$SRCR_{123}$ on the CM5 sensor chip, the deglycosylation was carried out by incubating the chip surface with a mixture containing a total reaction volume of 40 μl made up of 4 μl of 10× G7 reaction buffer, 4 μl of 10% Nonidet P-40, 4 μl of neuraminidase (Sigma), 18 μl of water, and 10 μl of *O*-glycosidase (New England Biolabs) and similarly following the manufacturer's protocols for endoglycosidase H (New England Biolabs). Later, the chip was sealed and incubated overnight at 37 °C. Subsequently, the chip was thoroughly washed with binding buffer (20 mM HEPES, 150 mM NaCl, 2.5 mM $CaCl_2$) to remove the deglycosylating enzymes and other remnants. Similar to the experimental procedure described above, in a separate experiment an off-chip deglycosylation of SRCRs was carried out and later checked to verify deglycosylation using MALDI-TOF MS analysis (data not shown). Binding studies with $FL^{AgI/II}$ and FL^{SspB} and their subfragments were then carried out as described above and regenerated as described in supplemental Table S2. All experiments were carried out in triplicate, and the kinetics of the association (K_A) and dissociation (K_D) rate constants were deduced using the 1:1 Langmuir kinetic model on the BIAevaluation software (36).

The utilization of a bivalent adherence model to elucidate the kinetics had inherent difficulties in clearly distinguishing affinities for each region, particularly for $FL^{AgI/II}$ and FL^{SspB}. In addition, the SRCR holding two distinct surfaces compounded the elucidation of individual kinetics, and presently there are no modeling protocols available to determine the individual affinities for such a system; therefore, for simplicity we have utilized a single site 1:1 Langmuir model. The larger χ^2 values observed for the full-length AgI/II and SspB are directly attributable to the multiple binding sites.

The concentration (*C* in micromolars) of analyte ($FL^{AgI/II}$ or FL^{SSpB} at 2 μM) that adhered to the immobilized ligand (*i*$SRCR_1$ and *i*$SRCR_{123}$) within the flow cell was calculated using the formula $C = (RU/M_r) \times (1/V)$, where RU is resonance unit (1 RU = 1 pg of bound protein); M_r is molecular weight of analyte, and *V* is volume of flow cell (1.2×10^{-10} liters).

Competition Adherence Assay—To determine whether AgI/II domains bound to the same site on SRCR domains, competitive binding SPR experiments were conducted in triplicate as described previously (13), where each fragment, 2 μM AgI/II (FL, A_3VP_1, or C_{123}) or SspB (FL, A_3VP_1, or C_{123}), was initially passed over the CM5 chip surface immobilized with either *i*$SRCR_1$, *i*$SRCR_{123}$, or SAG for 60 s to saturate available binding sites. The response curve of AgI/II or SspB fragment was first recorded, where the maximal RU (RU_1) was considered as the base line for the second injection, and thereafter, the competing fragment was injected, and its response was recorded as RU_2. The adherence of the second fragment was then calculated ($RU_2 - RU_1$) for all SPR competing assay as reported earlier (13).

ELISA—The binding between commercially synthesized (Think Peptides, Inc.) SRCRP2 peptide (QGRVEVLYRGSWGTVCK-(FAM)) with fluorescein amidite (FAM) at the carboxyl end and AgI/II homologs was analyzed. Briefly, AgI/II homologs (10 μg/well) in carbonate/bicarbonate buffer, pH 9.6, were coated on a black ELISA plate individually, washed with binding buffer (20 mM HEPES, pH 7.4, 150 mM NaCl, and 2.5 mM $CaCl_2$), and blocked with 3% nonfat dry skim milk. Serial dilution of the SRCRP2 peptide (200 μl) ranging from 0.03 to 1 mg/ml in binding buffer were then incubated with all fragments of AgI/II and SspB coated on wells for 3 h at room temperature. The coated wells without fluorescently labeled SRCRP2 peptides were used as controls. Later, the wells were washed with binding buffer, and the data were recorded at an excitation wavelength of 495 nm and emission at 519 nm using Synergy 2-multimode microplate reader and the results were then analyzed (Synergy, Inc.).

Adherence/Inhibition Studies—SRCRP2 peptide at different concentrations (5, 10, 50, 100, and 200 μM) was incubated with 2 μM each of FL, A_3VP_1, and C_{123} of AgI/II and SspB at room temperature for 3 h, and then their interaction with immobilized *i*$SRCR_1$ or *i*$SRCR_{123}$ on the CM5 chip was analyzed. Running buffer containing 20 mM HEPES, pH 7.4, 150 mM NaCl, and 2.5 mM $CaCl_2$ at 25 °C with a flow rate of 20 μl/min was used throughout the experiment. The CM5 chip was regenerated with buffer containing 1 M NaCl and 20 mM EDTA, pH 7.4, after each reaction cycle. Direct adherence of 200 μM SRCRP2 peptide alone served as the control, and all calculations on the adherence inhibition were assessed using the BIAevaluation software.

Aggregation Assay—Aggregation assays were performed as described earlier (34) with slight modifications. Briefly, *S. mutans* UA159 and *S. gordonii* DL1 cells were grown in TSY broth media (30 g/liter of trypticase soy broth and 0.5 g/liter yeast extract, pH 7.2) overnight at 37 °C in the presence of 5% CO_2. The bacteria were centrifuged at 5000 × *g* and washed with a buffer containing 20 mM HEPES, pH 7.4, 150 mM NaCl and resuspended to an approximate OD_{700} of 1. The bacterial suspension (900 μl) was mixed with 6 μl of 0.1 M $CaCl_2$ and 100 μl of SAG or *i*$SRCR_1$ or *i*$SRCR_{123}$ (10 μM) or SRCRP2 peptide (400 μg/ml). The aggregation of bacteria was then measured by recording OD_{700} over 60 min at 5-min intervals, where the buffer alone was used as control. All experiments were carried out at least five times, and the results were analyzed with one-way analysis of variance. Post hoc testing at $p < 0.05$ was considered statistically significant, and results were presented as the percentage of cells aggregated.

Confocal Microscopy—*S. mutans* UA159 and *S. gordonii* DL1 were grown overnight in TSY media on an eight-well LabTek chamber slide system (Sigma). The cells were fixed with 3% paraformaldehyde, washed with binding buffer (20 mM HEPES, pH 7.4, 150 mM NaCl, and 2.5 mM $CaCl_2$), and thereafter *i*$SRCR_1$ or *i*$SRCR_{123}$ (10 μM) was added to the cells and incubated for 60 min. The unbound SRCRs were removed by repeated washing using the binding buffer. Subsequently, Alexa

Fluor 488-conjugated anti-His tag antibody (EMD Millipore) (1:50 dilution) that can bind to the His tag on SRCRs was added. After 60 min of incubation, the unbound antibody was washed away thoroughly using binding buffer, and the chamber walls were gently removed. Coverslips were then mounted with 15 μl of Fluoromount-G with DAPI (Southern Biotech Inc.,) to stain bacterial nuclei and were sealed until ready to be imaged. The experiment without SRCRs served as control. All slides were imaged using a Leica SP1 UV confocal laser scanning microscope and a Zeiss LSM 710 confocal laser scanning microscope at the High Resolution Imaging Facility (University of Alabama at Birmingham).

Glycoprotein Staining and GC-MS Analysis of SRCRs Carbohydrates—The *i*SRCR$_1$ and *i*SRCR$_{123}$ proteins were electrophoretically separated on a 12.5% SDS-polyacrylamide gel and stained by glycoprotein staining kit (Pierce), where horseradish peroxidase (HRP) and soybean trypsin inhibitor were used as positive and negative controls, respectively. The glycosyl composition analysis of purified *i*SRCR$_1$ and *i*SRCR$_{123}$ was done by the preparation and gas chromatography-mass spectrometry (GC-MS) of trimethylsilyl methyl glycosides as described previously (37).

Circular Dichroism—Spectroscopic studies were carried out on an Olis DSM 100 circular dichroism spectrophotometer with a 0.2-mm path length quartz cell. Control recombinant *i*SRCR$_1$ or *i*SRCR$_{123}$ at a concentration of 1 mg/ml in a buffer containing 20 mM HEPES, pH 7.4, 150 mM NaCl at 22 °C was scanned between 200 and 260 nm, and the spectra was recorded (10 times). Similarly, the conformational changes of SRCRs on addition of different concentrations of calcium (1, 2.5, 10, and 100 mM) in binding buffer were analyzed. Using CONTIN/LL algorithm implemented in CDPRO (38), the protein secondary structures were analyzed.

Differential Scanning Calorimetry—The thermostability of SRCRs in the presence of calcium ions was analyzed using MicroCal MC-II differential scanning calorimeter (GE Healthcare) as described earlier (39). Briefly, *i*SRCR$_1$ or *i*SRCR$_{123}$ at a concentration of 1 mg/ml was mixed and incubated with different concentrations of $CaCl_2$ ranging from 0 to 100 mM to final volume of 400 μl of buffer containing 20 mM HEPES and 150 mM NaCl. Buffer without SRCRs served as control. Data were recorded with calorimetric scanning rates that ranged from 30 to 90 °C/h at 30 p.s.i. pressure. The data collected were analyzed for the unfolding temperature (T_m) and the calorimetric (ΔH_{cal}) and van't Hoff (ΔH_v) unfolding enthalpies using the Origin 7.0383 software package (MicroCal).

Analytical Ultracentrifugation—*i*SRCR$_1$ or *i*SRCR$_{123}$ (0.5 mg/ml) in a buffer containing 20 mM Tris, pH 8.0, 150 mM NaCl, and 1 mM EDTA were subjected to sedimentation velocity experiments on a Beckman Optima XL-A as described previously (12). Briefly, the samples were centrifuged to 45,000 rpm with the temperature maintained at 20 °C and absorbance at 280 nm across the cell recorded every 5 min. Using Sednterp, buffer density values of 1.0052 g/ml, protein partial specific volumes of 0.720 and 0.714 g/ml, and hydration values of 0.365 and 0.370 g/g for *i*SRCR$_1$ and *i*SRCR$_{123}$, respectively, were calculated (40, 41).

TABLE 1
Surface plasmon resonance studies

	Ligand	Analyte	k_a (1/Ms)	k_d (1/s)	K_A (1/M)	K_D (M)	Chi^2
S. mutans AgI/II	*i*SRCR$_1$	FL$^{AgI/II}$	1.67 x 10^5	8.07 x 10^{-4}	2.07 x 10^8	4.83 x 10^{-9}	15.40
		$A_3VP_1^{AgI/II}$	2.03 x 10^4	2.28 x 10^{-3}	8.88 x 10^6	1.13 x 10^{-7}	8.72
		$C_{123}^{AgI/II}$	8.98 x 10^3	1.02 x 10^{-5}	8.78 x 10^6	1.14 x 10^{-7}	8.41
	*i*SRCR$_1$ (Deglycosylated)	FL$^{AgI/II}$	1.41 x 10^4	4.71 x 10^{-3}	3.01 x 10^6	3.32 x 10^{-7}	19.42
		$A_3VP_1^{AgI/II}$	5.27 x 10^3	2.74 x 10^{-3}	1.92 x 10^6	5.20 x 10^{-7}	7.59
		$C_{123}^{AgI/II}$	1.18 x 10^3	24.6 x 10^{-3}	4.81 x 10^4	2.08 x 10^{-5}	9.31
	*i*SRCR$_{123}$	FL$^{AgI/II}$	1.04 x 10^5	7.60 x 10^{-4}	1.37 x 10^8	7.29 x 10^{-9}	18.90
		$A_3VP_1^{AgI/II}$	1.54 x 10^4	1.63 x 10^{-3}	9.47 x 10^6	1.06 x 10^{-7}	9.82
		$C_{123}^{AgI/II}$	8.50 x 10^3	1.56 x 10^{-4}	5.47 x 10^7	1.83 x 10^{-8}	10.50
	*i*SRCR$_{123}$ (Deglycosylated)	FL$^{AgI/II}$	3.16 x 10^3	4.64 x 10^{-4}	6.82 x 10^6	1.47 x 10^{-7}	18.20
		$A_3VP_1^{AgI/II}$	4.07 x 10^3	3.33 x 10^{-3}	1.22 x 10^6	8.18 x 10^{-7}	6.53
		$C_{123}^{AgI/II}$	3.01 x 10^3	6.58 x 10^{-3}	4.58 x 10^5	2.18 x 10^{-6}	7.45
S. gordonii SspB	*i*SRCR$_1$	FL^{SspB}	9.26 x 10^3	2.24 x 10^{-3}	4.13 x 10^6	2.42 x 10^{-7}	14.01
		$A_3VP_1^{SspB}$	9.78 x 10^4	9.97 x 10^{-4}	5.76 x 10^6	1.74 x 10^{-7}	9.35
		C_{123}^{SspB}	7.03 x 10^3	3.33 x 10^{-3}	2.11 x 10^6	4.73 x 10^{-7}	6.11
	*i*SRCR$_1$ (Deglycosylated)	FL^{SspB}	2.86 x 10^4	4.16 x 10^{-3}	6.88 x 10^6	1.45 x 10^{-7}	6.51
		$A_3VP_1^{SspB}$	3.70 x 10^4	12.5 x 10^{-3}	2.96 x 10^6	3.38 x 10^{-7}	8.25
		C_{123}^{SspB}	1.90 x 10^4	20.7 x 10^{-3}	9.21 x 10^5	1.09 x 10^{-6}	1.04
	*i*SRCR$_{123}$	FL^{SspB}	1.97 x 10^4	9.51 x 10^{-4}	2.08 x 10^7	4.82 x 10^{-8}	15.11
		$A_3VP_1^{SspB}$	7.91 x 10^4	13.7 x 10^{-4}	5.76 x 10^6	1.74 x 10^{-7}	9.91
		C_{123}^{SspB}	8.43 x 10^3	2.21 x 10^{-3}	3.82 x 10^6	2.62 x 10^{-7}	6.02
	*i*SRCR$_{123}$ (Deglycosylated)	FL^{SspB}	1.83 x 10^4	2.59 x 10^{-3}	7.06 x 10^6	1.42 x 10^{-7}	4.11
		$A_3VP_1^{SspB}$	7.80 x 10^4	56.7 x 10^{-3}	1.38 x 10^6	7.27 x 10^{-7}	7.79
		C_{123}^{SspB}	2.42 x 10^3	15.1 x 10^{-3}	1.61 x 10^5	6.22 x 10^{-6}	2.93
	SAG	FL^{SspB}	3.20 x 10^5	1.97 x 10^{-3}	1.63 x 10^8	6.15 x 10^{-9}	14.30
		$A_3VP_1^{SspB}$	5.73 x 10^4	4.72 x 10^{-3}	1.22 x 10^7	8.21 x 10^{-8}	9.51
		C_{123}^{SspB}	2.72 x 10^4	2.16 x 10^{-3}	1.26 x 10^7	7.96 x 10^{-8}	8.33

RESULTS

Adherence Assays and Quantitation—The adherence affinities between immobilized *i*SRCRs and the analytes FL, A_3VP_1, and C_{123} of AgI/II and SspB are summarized in Table 1 and supplemental Fig. S2, *A–C*. All fragments of AgI/II and SspB interact with nanomolar affinity to immobilized SRCRs. Although FL$^{AgI/II}$ and FL^{SspB} displayed similar affinities with *i*SRCR$_1$ and *i*SRCR$_{123}$, the quantity of protein that adhered to *i*SRCR$_{123}$ was higher (16% for FL$^{AgI/II}$ and 43% for FL^{SspB}) than that of *i*SRCR$_1$ (supplemental Fig. S3).

Competitive Binding Experiments—FL$^{AgI/II}$ was able to inhibit the binding of $A_3VP_1^{AgI/II}$ and $C_{123}^{AgI/II}$ by 46 and 36% respectively, whereas FL^{SspB} inhibited $A_3VP_1^{SspB}$ and C_{123}^{SspB} by 54 and 23% with immobilized *i*SRCR$_1$ (Fig. 3). In all other cases, A_3VP_1 or C_{123} of AgI/II and SspB did not significantly inhibit the adherence of each other. These results validate that a single SRCR domain contains the two distinct surfaces that specifically bind A_3VP_1 as well as C_{123} fragments of the AgI/II homologs.

Similar inhibition was observed with immobilized *i*SRCR$_{123}$ domains where FL$^{AgI/II}$ inhibited the binding of $A_3VP_1^{AgI/II}$ and $C_{123}^{AgI/II}$ by 44 and 25%. However, FL^{SspB} had limited inhibitory effects with immobilized *i*SRCR$_{123}$, where A_3VP_1 and C_{123} displayed 68 and 76% inhibition respectively. This shows that AgI/II and SspB are different in their adherence characteristics, although they are highly homologous (57% identity and 70% homology).

The results from the competitive adherence experiments conclusively provide evidence for multiple adherence sites within a single SRCR domain and have thus narrowed down

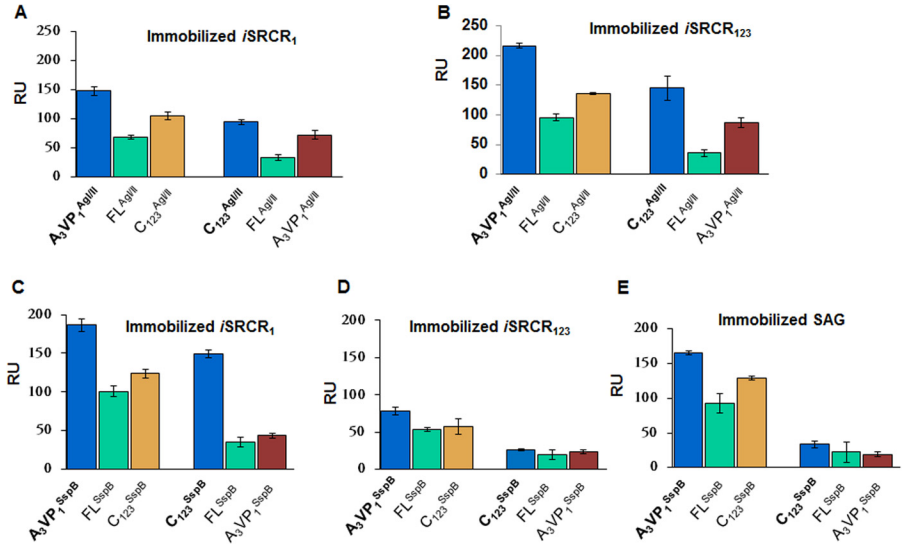

FIGURE 3. Competition experiments with $FL^{AgI/II}$, $A_3VP_1^{AgI/II}$, and $C_{123}^{AgI/II}$ were conducted with immobilized *i*$SRCR_1$ (*A*) and immobilized *i*$SRCR_{123}$ (*B*) to determine the multiple adherence sites of the SRCRs. Although the direct adherence of the fragment is shown in *bold* (such as $A_3VP_1^{AgI/II}$), the observed adherence inhibition in the presence of competing fragments ($FL^{AgI/II}$ and $C_{123}^{AgI/II}$) are plotted in subsequent *bar graphs*. Similarly, the competition of FL^{SspB}, $A_3VP_1^{SspB}$, and C_{123}^{SspB} with immobilized *i*$SRCR_1$, *i*$SRCR_{123}$, and SAG are shown in *C–E*. All experiments were carried out in triplicate, and the *error bars* represent standard deviations.

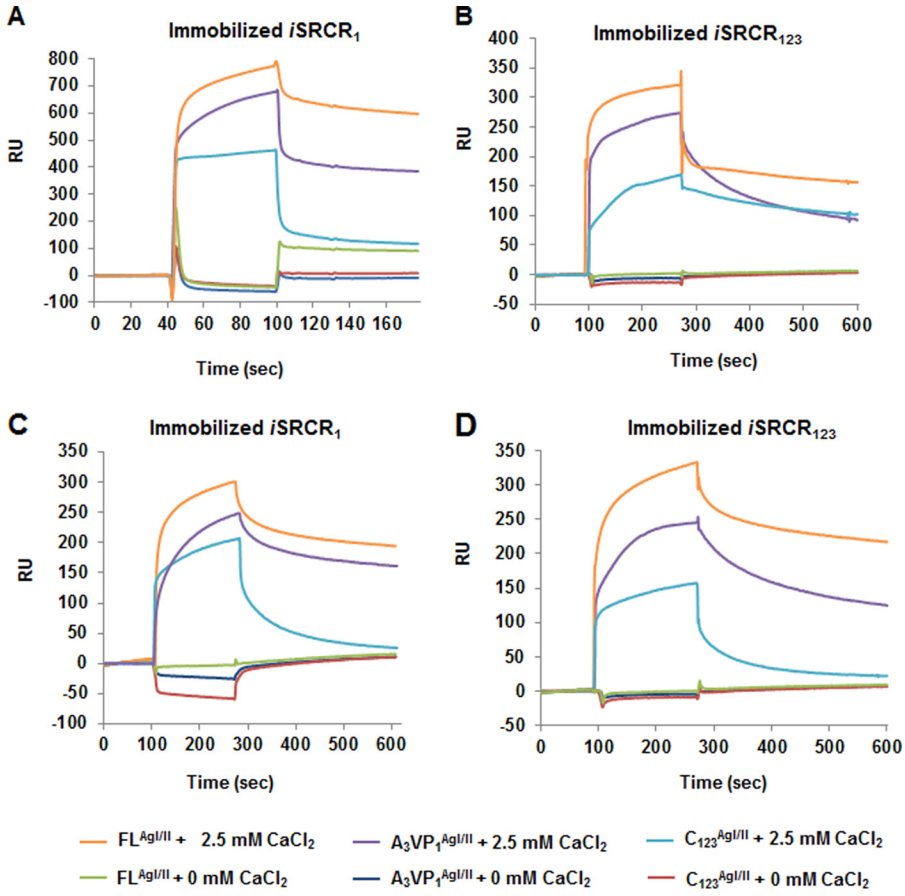

FIGURE 4. Illustrated here are the calcium-mediated adherences of (2 μM) AgI/II of *S. mutans* with *i*$SRCR_1$ (*A*) and *i*$SRCR_{123}$ (*B*) on a CM5 sensor chip. The adherence of AgI/II fragments was observed only in the presence of calcium. Devoid of calcium, AgI/II did not adhere to SRCRs. A similar result was observed with SspB of *S. gordonii* (*C* and *D*).

the region of adherence to the SRCR domains of GP340. This concurs with our earlier observation of multiple sites on SAG (12).

Role of Calcium (Calcium-mediated Adherence/Stability)—In the absence of calcium, there was no adherence between AgI/II homologs and SRCRs (Fig. 4, *A–D*). In the presence of

TABLE 2
CD analysis of SRCRs at various calcium concentrations

$CaCl_2$	Helix (%)		β-Sheet (%)		Turn (%)		Random coil (%)	
	i$SRCR_1$	*i*$SRCR_{123}$	*i*$SRCR_1$	*i*$SRCR_{123}$	*i*$SRCR_1$	*i*$SRCR_{123}$	*i*$SRCR_1$	*i*$SRCR_{123}$
0 mM	15.9	14.8	28.3	22.9	20.4	18.2	35.4	44.2
1 mM	6.3	5.9	34.2	34.4	24.0	20.3	35.5	37.3
2.5 mM	6.6	6.8	37.4	34.2	24.2	20.4	31.9	38.6
10 mM	6.8	5.4	35.9	34.9	24.3	19.5	33.0	40.3
100 mM	7.2	4.0	39.3	36.2	22.2	18.8	31.3	41.1

TABLE 3
Differential scanning calorimetric analysis of SRCRs at various calcium concentrations

Samples	Calorimetric enthalpy (ΔH_{cal})	Van't Hoff enthalpy (ΔH_V)	T_m
	Cal/mol	*Cal/mol*	°C
i$SRCR_1$	$5.703 \times 10^4 \pm 216$	$6.016 \times 10^4 \pm 281$	56.5
i$SRCR_1$ + 2.5 mM $CaCl_2$	$7.828 \times 10^4 \pm 280$	$8.455 \times 10^4 \pm 374$	78.1
i$SRCR_1$ + 10 mM $CaCl_2$	$6.708 \times 10^4 \pm 412$	$11.17 \times 10^4 \pm 854$	86.4
i$SRCR_1$ + 100 mM $CaCl_2$	$9.736 \times 10^4 \pm 1.55 \times 10^3$	$11.11 \times 10^4 \pm 2.24 \times 10^3$	92.8

TABLE 4
Glycan profile analysis of *i*$SRCR_1$ and *i*$SRCR_{123}$

i$SRCR_1$			*i*$SRCR_{123}$		
Sugars	Carbohydrates (nmol/ mg protein)	Mole (%)	Sugars	Carbohydrates (nmol/mg protein)	Mole (%)
Xylose	23.33	3.45	Fucose	21.12	1.47
Glucuronic acid	85.13	12.58	Xylose	16.26	1.14
Mannose	156.28	23.10	Glucuronic acid	36.92	2.58
Galactose	108.99	16.11	Mannose	815.48	56.94
Glucose	1.50	0.22	Galactose	112.33	7.84
N-Acetylgalactosamine	287.56	42.51	Glucose	1.79	0.13
N-Acetylglucosamine	13.68	2.02	N-Acetylgalactosamine	392.86	27.43
			N-Acetylglucosamine	35.46	2.48
SUM	676.47	100.00	SUM	1432.22	100.00
Sample (mg)			1.00	1.00	
Carbohydrates (mg)			0.11	0.25	
Carbohydrates (%)			11.41	25.32	

calcium, CD spectra had recorded a significant reduction in α-helices that was correspondingly compensated with an increase in β-sheet content (Table 2), whereas no such changes were observed with AgI/II or SspB (data not shown). Upon calcium addition, the stability (thermal unfolding) of *i*$SRCR_1$ increased in a dose-dependent manner (Table 3), and at 100 mM $CaCl_2$, the SRCR domain unfolded at an uncharacteristically surprising 90 °C. Although the thermal unfolding curves of *i*$SRCR_1$ were simple and easy to interpret, *i*$SRCR_{123}$ was more complex to interpret as it involved multiple domains (data not shown).

The homologous structures of SRCR domains from both group A (with six cysteines) and group B (with eight cysteines) have been determined (42, 43); however, to date there are no crystal structures of the SRCR domains of GP340. Both *i*$SRCR_1$ and *i*$SRCR_{123}$ domains possess similar secondary structures compared with the solved crystal structures PDB2JA4, PDB1BY2, and PDB1P57 (23, 42, 44), thus indicating a possible adoption of similar SRCR folds.

Effect of Carbohydrates on the Adherence of AgI/II—The presence of glycosylation on *i*$SRCR_1$ and *i*$SRCR_{123}$ was initially confirmed using glycoprotein staining (supplemental Fig. S4). Further glycan profile analysis of both *i*$SRCR_1$ and *i*$SRCR_{123}$ indicated that they are predominantly *O*-glycosylated with Galβ1–3-GalNac and mannose carbohydrates (Table 4). Deglycosylation of *i*$SRCR_1$ and *i*$SRCR_{123}$ by *O*-glycosidases did not affect the adherence characteristics of $A_3VP_1^{AgI/II}$ but decreased the adherence of the $C_{123}^{AgI/II}$ by 2 orders of magnitude (Table 1), implicating the involvement of domains closer to the cell surface in carbohydrate binding. Similar results were observed with C_{123}^{SspB}. Although *O*-glycosidases had profound effects on the adherence kinetics, endoglycosidase H (*N*-glycosidase) did not have any measurable effect (data not shown).

SRCRP2 (Bikker Peptide)—Initial ELISAs (Fig. 5*A*) demonstrated the adherence of the SRCRP2 peptide to AgI/II, SspB, and their subfragments. When incubated at low concentration (5 μM) with $FL^{AgI/II}$ and $A_3VP_1^{AgI/II}$, the SRCRP2 peptide improved the adherence by 8 and 13% respectively to *i*$SRCR_1$ (data not shown) and 8 and 16% respectively to *i*$SRCR_{123}$, whereas $C_{123}^{AgI/II}$ had no changes in adherence (Fig. 5*B*). Only FL^{SspB} improved the adherence by 97% with *i*$SRCR_{123}$ at lower concentration (5 μM of SRCRP2 peptide), whereas $A_3VP_1^{SspB}$ and C_{123}^{SspB} did not alter the adherence characteristics to either *i*$SRCR_1$ (data not shown) or *i*$SRCR_{123}$ (3 and 5%), respectively (Fig. 5*B*). Also, the SRCRP2 alone (control) did not show any binding with SRCRs. These results indicated that SRCRP2 peptide does not inhibit the adherence of AgI/II and SspB to *i*$SRCR_1$ and *i*$SRCR_{123}$ and that the adherence site was different from that of the aggregation sites present on AgI/II and SspB.

SRCR Self-adhesion—Interaction of SRCRs with each other was tested using SPR. The *i*$SRCR_1$ and *i*$SRCR_{123}$ strongly interacted with each other. Analytes *i*$SRCR_1$ ($K_D = 1.13 \times 10^{-10}$ M) and *i*$SRCR_{123}$ ($K_D = 5.68 \times 10^{-9}$ M) demonstrated high affinity with immobilized *i*$SRCR_1$. Similarly, analytes *i*$SRCR_1$ ($K_D = 1.2 \times 10^{-9}$ M) and *i*$SRCR_{123}$ ($K_D = 6.72 \times 10^{-9}$ M) interacted with immobilized *i*$SRCR_{123}$ with nanomolar affinities (Fig. 6, *A–D*). These results showed that the SRCRs have self-adhesion property as well.

Aggregation Assays—In the presence of *i*$SRCR_{123}$, 69% of *S. mutans* and 48% of *S. gordonii* aggregated, whereas *i*$SRCR_1$ aggregated 17% of *S. mutans* and 12% of *S. gordonii* (Fig. 7, *A* and *B*). The positive control SAG aggregated *S. mutans* by 74% and *S. gordonii* by 72%. Earlier studies with the consensus peptide, SRCRP2 derived from SRCR domains, aggregated a variety of bacteria (17, 31); however, in this study compared with *i*$SRCR_{123}$, the SRCRP2 peptide displayed very limited aggregation with *S. mutans* (13%) and *S. gordonii* (11%) similar to that of a single SRCR domain. Even at higher concentrations, the

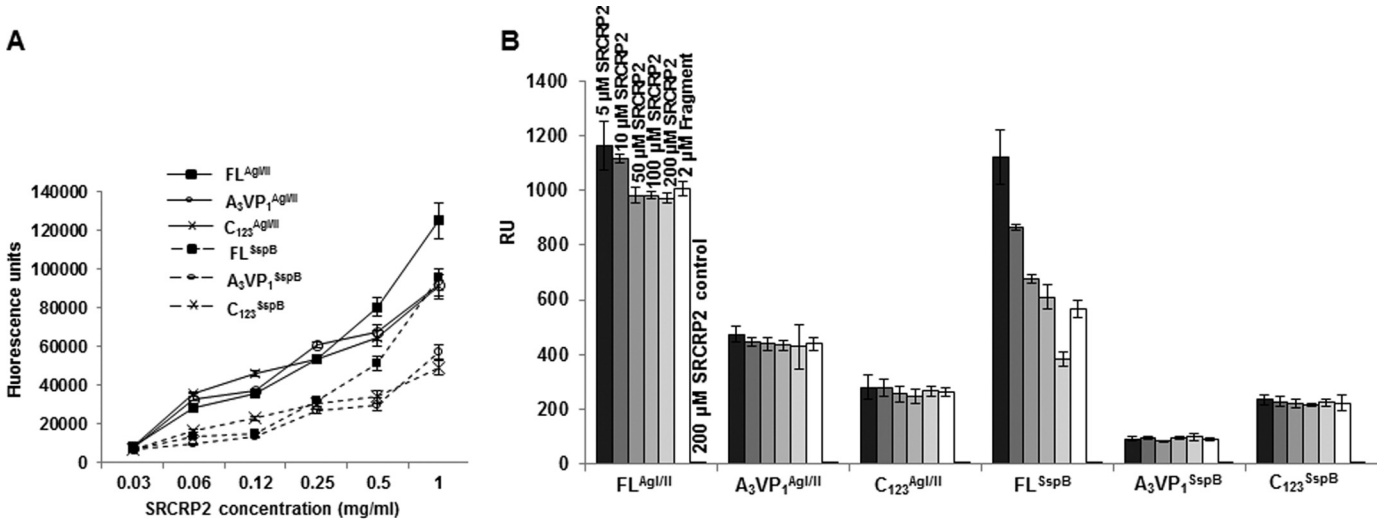

FIGURE 5. *A*, these curves illustrate the direct adherence of SRCRP2 peptide to $FL^{AgI/II}$ $A_3VP_1^{AgI/II}$, and $C_{123}^{AgI/II}$ of *S. mutans* (*bold lines*) as well as FL^{SspB}, $A_3VP_1^{SspB}$, and C_{123}^{SspB} of *S. gordonii* (*dotted lines*). Fluorescein-tagged SRCRP2 (FAM) was serially diluted (0.03–1 mg/ml), and its interaction with immobilized AgI/II and SspB and their subfragments was measured at OD_{519}. The results illustrated that the SRCRP2 peptide adheres well with AgI/II and SspB. *B*, adherence/inhibition of $FL^{AgI/II}$ and FL^{SspB} and subfragments (2 μM) in the presence of SRCRP2 peptide at various concentrations (0.005 to 0.200 mM) with immobilized $iSRCR_{123}$. In control experiments, SRCRP2 peptide alone does not display any measurable interaction with $iSRCR_{123}$. More importantly SRCRP2 does not inhibit the adherence of AgI/II and SspB (and their subfragments) to the SRCRs. Surprisingly, SRCRP2 increased the adhesiveness of FL^{SspB} confounding us, as it could be interpreted as nonspecific adherence/aggregation.

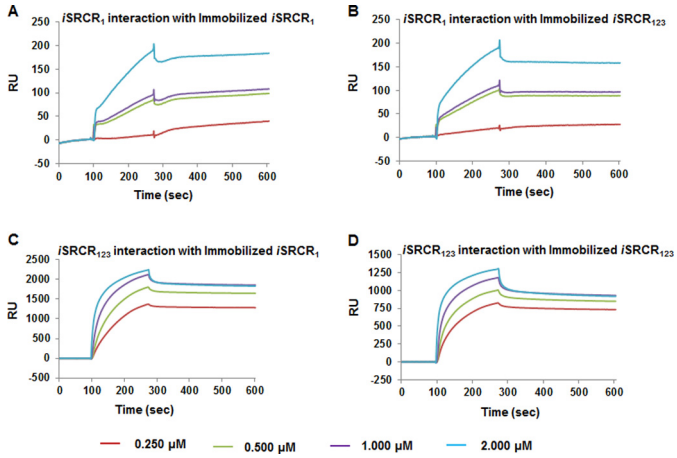

FIGURE 6. **Self-interactions of SRCR domains at various concentrations (0.250–2 μM) with immobilized $iSRCR_1$ (*A* and *C*) and $iSRCR_{123}$ (*B* and *D*) on CM5 sensor chip were analyzed using BIA-Evaluation software.** The analytes $iSRCR_1$ and $iSRCR_{123}$ demonstrated nanomolar affinity interaction with SRCRs, clearly indicating the self-adhesion property among SRCRs.

SRCRP2 peptide did not aggregate *S. mutans* and *S. gordonii* (data not shown).

Confocal Microscopy—The Z view of the confocal microscopy pictures show the adherence of SRCRs to the upper surface (surface proteins) of immobilized *S. mutans* UA159 and *S. gordonii* DL1 cells (Fig. 8, *A* and *B*). From the X-Y panel view, it is noticeable that $iSRCR_1$ adhered poorly compared with $iSRCR_{123}$, underscoring that multiple SRCR domains have better adherence capability compared with that of a single SRCR domain.

Analytical Ultracentrifugation—We sought to answer the question of the spatial organization of the SRCR domains, particularly whether they might be elongated similarly to AgI/II through ultracentrifugation experiments. From their observed frictional ratios ($iSRCR_1$ = 1.59 and $iSRCR_{123}$ = 1.80), resultant prolate ellipsoid ratios ($iSRCR_1$ = 7.18 and $iSRCR_{123}$ = 10.36), and calculated dimensions ($iSRCR_1$ = 12.60 × 1.75 nm and $iSRCR_{123}$ = 22.08 × 2.13 nm), it is evident that both $iSRCR_1$ and $iSRCR_{123}$ will have extended structures (Table 5). However, these are not extended as linear rigid structures but exist in a flexible nonlinear conformation forming curvy tertiary structures.

DISCUSSION

Oral streptococci primarily attach to tooth-immobilized GP340 via AgI/II homologs and subsequently colonize and infect the host (19, 45). For the past 3 decades, this interaction has been studied using GP340 extracted from the saliva of either single or multiple donors who have inherent allelic variability (30, 46, 47). For the first time in this study using recombinantly expressed SRCR domains of GP340 (*Drosophila* expression system), we established a benchmark and elucidated the intricate components involved in this bacterial adhesion.

Nanomolar affinity interactions between the SRCRs and AgI/II homologs (Table 1 and supplemental Fig. S2, *A–C*) were deduced from SPR data. The adherence kinetics of the C_{123}^{SspB} (present near cell the wall) had distinctive sensorgrams, where they did not remain bound to the immobilized SAG or SRCR domains (supplemental Fig. S2*C*). Overall, these results imply that SAG-binding protein AgI/II of pathogenic *S. mutans* contains a locking mechanism to remain bound, whereas the C-terminal region of the commensal *S. gordonii* SspB does not. In isothermal titration calorimetry experiments (supplemental Fig. S5), the affinity between the AgI/II and SRCR in solution was in the micromolar range and indicated that the nature of the interaction is very different in solution compared with an immobilized state.

This study also demonstrates that the adherence surfaces for A_3VP_1 and C_{123} of AgI/II are contained within a single SRCR domain, and it is therefore the minimal adherence region (Fig. 3, *A–E*).

The concentration of calcium within the oral cavity has been estimated to be between 1.2 and 2.8 mmol/liter, and using sim-

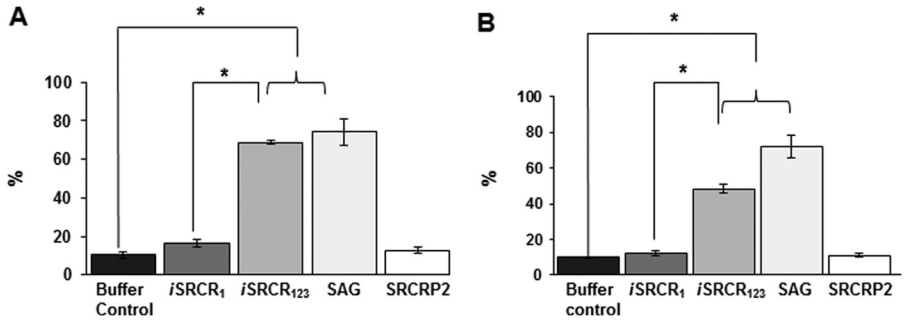

FIGURE 7. **Aggregation of *S. mutans* UA159 (*A*) and *S. gordonii* DL1 (*B*) cells in the presence of *i*SRCRs, SAG, and SRCRP2 peptide was analyzed.** The results are plotted as percentage of aggregation measured at OD_{700} at 5-min intervals for 1 h. Bacterial cells in buffer alone were used as control. Differences in aggregation detected between groups were analyzed using one-way analysis of variance, where *, $p < 0.05$ was considered significant, and *error bars* represent the standard deviation.

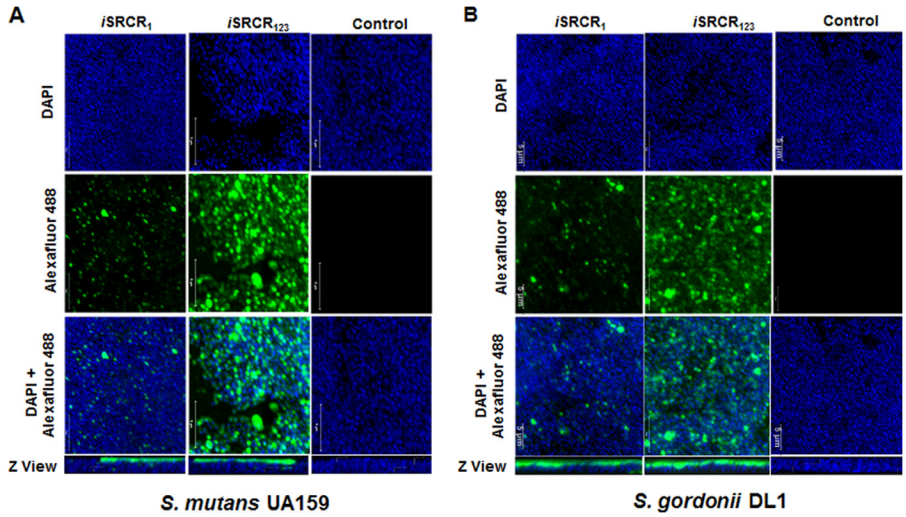

FIGURE 8. **Interaction between *S. mutans* UA159 (*A*) and *S. gordonii* DL1 (*B*) cells with $iSRCR_1$ and $iSRCR_{123}$ was analyzed using confocal microscopic images.** The images display *S. mutans* and *S. gordonii* cells stained with DAPI (*blue*) and anti-His tag Alexa Fluor 488 antibody (*green*). The observed green fluorescence depicts the binding of $iSRCR_1$ and $iSRCR_{123}$ to *S. mutans* and *S. gordonii,* whereas the control *S. mutans* and *S. gordonii* were counterstained by DAPI alone. Also, it is evident from the images that $iSRCR_{123}$ adhered more profoundly than $iSRCR_1$.

TABLE 5

Analytical ultracentrifugation analysis of the SRCRs

r.m.s.d. means root mean square deviation.

Construct	Theoretical mass	Fit mass	Fit r.m.s.d.	S20	f/f_0	Stokes radius	a/b (oblate)	a/b (prolate)	Oblate ellipsoid	Prolate ellipsoid
	Da	*Da*	*OD*	*S*		*nm*			*nm* × *nm*	*nm* × *nm*
$iSRCR_1$	14906	17031	0.0054	1.508	1.59	2.71	7.94	7.18	6.73 × 0.84	12.60 × 1.75
$iSRCR_{123}$	42549	51357	0.0062	2.792	1.80	4.43	11.67	10.36	10.54 × 0.90	22.08 × 2.13

ilar concentrations, we discovered that calcium induces secondary structural changes (Table 2) and increases the thermal stability of the SRCRs (Table 3). Because the oral cavity is subject to environmental changes, including pH and temperature changes (hot and cold food and beverages), perhaps the observed thermal stability could be a direct consequence of evolution. It would be interesting to see whether the SRCR domains from sea urchin, which has 57% sequence identity with human GP340 SRCR domain, possess these thermal properties that would directly link it to evolution of the SRCR domains within the human oral cavity. In SPR experiments (supplemental Fig. S6), calcium induced a large change in RUs while interacting with the immobilized SRCRs. Such phenomena have been observed in other proteins that endure calcium-induced structural and conformational changes (48). This opens up the possibility that the SRCRs undergo a distinct conformational change in the immobilized state, to which the bacterial AgI/II homologs adhere with nanomolar affinity, whereas in a solution state they adhere with micromolar affinity (supplemental Fig. S5). Physiologically, this could represent an evolution of streptococci in the oral cavity, where GP340 (being an innate immunity molecule) would aggregate the microbes and clear them into the gut, and to survive, bacteria have developed specific higher affinity to the tooth-immobilized conformation of GP340.

The positive glycostaining (supplemental Fig. S4) and the glycan profile analysis of recombinant SRCRs (Table 4) indicated that they are predominantly *O*-glycosylated. Deglycosylation of SRCRs with *O*-glycanase reduced the adherence affinity (Table 1), and therefore, for the first time we have now quantitatively determined that the high affinity interactions observed between AgI/II homologs and SRCRs/SAG is directly attributed to the carbohydrate adherence.

Compared with iSRCR$_1$ and iSRCR$_{123}$, the SRCRP2 peptide (Fig. 5*B*) showed limited aggregation with AgI/II homologs. In addition, SRCRP2 did not offer significant inhibition. There are two possibilities, one is that the aggregation site is different from that of the adhesion in AgI/II homologs, or this could be interpreted as nonspecific adherence by the peptide. We lean toward nonspecific adherence as SRCRP2 increased the adhesiveness of only FL^{SspB}. These results now demonstrate that the peptide does not aggregate well nor does it inhibit the SRCR/GP340-binding motif/site on AgI/II homologs.

Confocal microscopic images (Fig. 8, *A* and *B*) and aggregation assays (Fig. 7, *A* and *B*) show that iSRCRs bind to *S. mutans* and *S. gordonii* cells, where iSRCR$_{123}$ attaches extensively compared with iSRCR$_1$. Detailed SPR analysis based on protein adherence to chip surface indicated higher amounts of FL$^{AgI/II}$ and FL^{SspB} adhered to immobilized iSRCR$_{123}$ than iSRCR$_1$ (supplemental Fig. S3). Based on these observations, we conclude that longer tandem SRCR domains would more efficiently agglutinate various bacteria. With GP340 being an innate immunity molecule, the number of tandem repeats it takes to efficiently agglutinate bacteria could have been evolutionarily determined, and it is interesting to note that in humans GP340 contains 14 SRCR domains, of which 13 are tandem repeats, whereas in other vertebrates the number of tandem repeats are comparatively lower (26, 27).

One surprising result that came out of these studies is that the SRCR domains self-associate with nanomolar affinities, thus indicating that this association is highly specific, as nonspecific interactions traditionally appear to fall within the micromolar range (Fig. 6, *A*–*D*). GP340 is known to exist as a higher order complex, and these aggregates could be as large as 5000 kDa (19, 49). Thus far, the aggregation property of GP340 has been attributed to the ZP domain; as in other mammalian proteins, the ZP domain was shown to be involved in self-aggregation (50). Furthermore, the tertiary architecture analysis of tandem SRCR domains indicate that they may not strictly form a linear elongated structure (Table 5) but could form a curvy centipede-like extended structure, similar to that observed in electron microscopy images of GP340 (28). Combined together, these results open up several possible models for bacterial aggregation/adherence, wherein one potential model could simulate the bacterial proteins to be sandwiched between two SRCR domains (GP340s) (Fig. 9).

Earlier studies have shown that the SRCR domains of GP340 play a pivotal role in mediating HIV adhesion/clearance through GP120 (16, 51). Although GP340 acted as a clearance mechanism in the oral cavity, the case was very different on the vaginally derived GP340, which is immobilized on the cell surface, where this was shown to mediate transcytosis from apical to basolateral surface in both genital tract epithelial cells in culture and with endocervical tissue (52). Similarly, in SPR experiments, immobilized SRCRs adhere tightly to AgI/II homologs, and in the fluid phase SRCRs aggregate *S. mutans* and *S. gordonii*, a double-faceted property, where on the one hand it acts as a portal of entry for microbes while immobilized and on the other hand as a clearance mechanism within the oral cavity in fluid state. This property indicates that SRCRs could possibly adopt different secondary structural conformations in fluid and immobilized states, and this conformation could be induced by calcium ions.

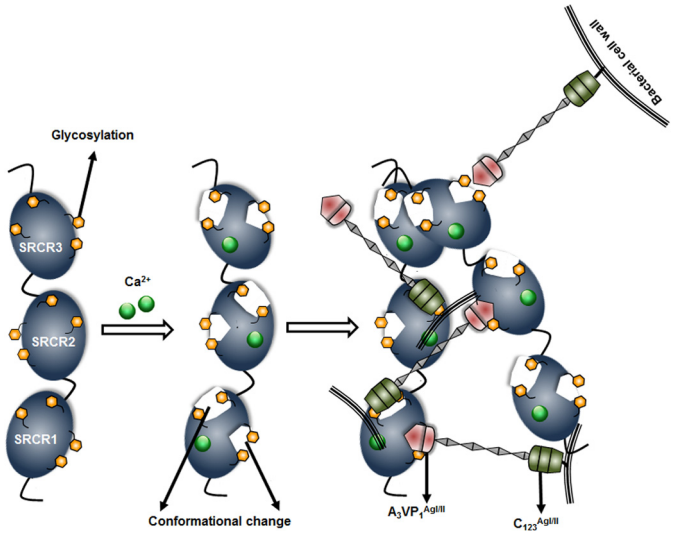

FIGURE 9. **Schematic model displaying the conformational change on the SRCR domains of GP340 in the presence of calcium, and particularly implicating the role of glycosylation in this high affinity adherence to AgI/II homologs.** The model also includes the possible self-association of the SRCR domains that could potentially sandwich AgI/II homologs of oral streptococci.

Summarizing our findings, we report that the minimal adherence region is restricted to a single SRCR domain, which carries the two distinct surfaces that adhere to A_3VP_1 as well as C_{123} of both AgI/II and SspB. Better adherence and aggregation of bacteria are observed with increasing numbers of SRCR domains. These SRCR domains attain stability in the presence of calcium, and calcium mediates structural changes that are essential for the adherence of AgI/II homologs. Furthermore, glycosylations play a significant role in the adherence to AgI/II and SspB. Interestingly, the SRCRs self-associate and the tandem domains may adopt a curvy centipede-like structure. Although there are similarities in the binding of AgI/II and SspB, there are certainly distinct differences pointing toward species specificity in their adherence.

Overall, these results now point to the fact that focusing on the SRCRs and elucidating the molecular motifs involved in adherence would aid in the development of interventional therapeutics. Such studies could potentially result in the identification and development of small molecule inhibitors or passive immunization therapies that could impede oral streptococcal adherence to tooth surfaces and alleviate the global burden of dental caries.

Acknowledgments—We acknowledge the X-ray Core, Comprehensive Cancer Center, and High Resolution Imaging Facilities at the University of Alabama at Birmingham. We are grateful to Dr. Christie Brouillette and Dr. Peter Prevelige for CD, differential scanning calorimetry, and analytical ultracentrifugation instrumentation. We thank Dr. L. Jeannine Brady for SAG and Dr. Poustka for the DMBT1 (GP340) gene template. We also thank Brian Sharon, Manisha Patel, and Shaan Khaled for protein purifications and Zhengrong Yang and Matthew Larson for discussions.

REFERENCES

1. Lehner, T., Russell, M. W., and Caldwell, J. (1980) Immunization with a purified protein from *Streptococcus mutans* against dental caries in rhesus monkeys. *Lancet* **1,** 995–996
2. Russell, M. W., Childers, N. K., Michalik, S. M., Smith, D. J., and Taanman, M. A. (2004) A Caries vaccine? The state of the science of immunization against dental caries. *Caries Res.* **38,** 230–235
3. Robinette, R. A., Olli, M. W., McArthur, W. P., and Brady, L. J. (2011) A therapeutic anti-*Streptococcus mutans* monoclonal antibody used in human passive protection trials influences the adaptive immune response. *Vaccine* **29,** 6292–6300
4. El-Sabens, A., Demuth, D. R., and Lamont, R. J. (2001) Regulation of *Streptococcus gordonii* SspB by the SspA gene product. *Infect. Immun.* **69,** 6520–6522
5. Lamont, R. J., El-Sabens, A., Park, Y., Cook, G. S., Costantin, J. W., and Demuth, D. R. (2002) Role of the *Streptococcus gordonii* SspB protein in the development of *Porphyromonas gingivalis* biofilms on streptococcal substrates. *Microbiology* **148,** 1627–1636
6. Demuth, D. R., Duan, Y., Brooks, W., Holmes, A. R., McNab, R., and Jenkinson, H. F. (1996) Tandem genes encode cell-surface polypeptides SspA and SspB which mediate adhesion of the oral bacterium *Streptococcus gordonii* to human and bacterial receptors. *Mol. Microbiol.* **20,** 403–413
7. Chung, W. O., Demuth, D. R., and Lamont, R. J. (2000) Identification of a *Porphyromonas gingivalis* receptor for the *Streptococcus gordonii* SspB protein. *Infect. Immun.* **68,** 6758–6762
8. Brady, L. J., Maddocks, S. E., Larson, M. R., Forsgren, N., Persson, K., Deivanayagam, C. C., and Jenkinson, H. F. (2010) The changing faces of *Streptococcus* antigen I/II polypeptide family adhesins. *Mol. Microbiol.* **77,** 276–286
9. Nobbs, A. H., Lamont, R. J., and Jenkinson, H. F. (2009) *Streptococcus* adherence and colonization. *Microbiol. Mol. Biol. Rev.* **73,** 407–450
10. Ericson, T., and Rundegren, J. (1983) Characterization of a salivary agglutinin reacting with a serotype c strain of *Streptococcus mutans*. *Eur. J. Biochem.* **133,** 255–261
11. Mollenhauer, J., Wiemann, S., Scheurlen, W., Korn, B., Hayashi, Y., Wilgenbus, K. K., von Deimling, A., and Poustka, A. (1997) DMBT1, a new member of the SRCR superfamily, on chromosome 10q25.3–26.1, is deleted in malignant brain tumours. *Nat. Genet.* **17,** 32–39
12. Larson, M. R., Rajashankar, K. R., Patel, M. H., Robinette, R. A., Crowley, P. J., Michalek, S., Brady, L. J., and Deivanayagam, C. (2010) Elongated fibrillar structure of a streptococcal adhesin assembled by the high-affinity association of α- and PPII-helices. *Proc. Natl. Acad. Sci. U.S.A.* **107,** 5983–5988
13. Larson, M. R., Rajashankar, K. R., Crowley, P. J., Kelly, C., Mitchell, T. J., Brady, L. J., and Deivanayagam, C. (2011) Crystal structure of the C-terminal region of *Streptococcus mutans* antigen I/II and characterization of salivary agglutinin adherence domains. *J. Biol. Chem.* **286,** 21657–21666
14. Deivanayagam, C. C., Wann, E. R., Chen, W., Carson, M., Rajashankar, K. R., Höök, M., and Narayana, S. V. (2002) A novel variant of the immunoglobulin fold in surface adhesins of *Staphylococcus aureus*: crystal structure of the fibrinogen-binding MSCRAMM, clumping factor A. *EMBO J.* **21,** 6660–6672
15. Leito, J. T., Ligtenberg, A. J., van Houdt, M., van den Berg, T. K., and Wouters, D. (2011) The bacteria binding glycoprotein salivary agglutinin (SAG/gp340) activates complement via the lectin pathway. *Mol. Immunol.* **49,** 185–190
16. Wu, Z., Golub, E., Abrams, W. R., and Malamud, D. (2004) gp340 (SAG) binds to the V3 sequence of gp120 important for chemokine receptor interaction. *AIDS Res. Hum. Retroviruses* **20,** 600–607
17. Bikker, F. J., Ligtenberg, A. J., Nazmi, K., Veerman, E. C., van't Hof, W., Bolscher, J. G., Poustka, A., Nieuw Amerongen, A. V., and Mollenhauer, J. (2002) Identification of the bacteria-binding peptide domain on salivary agglutinin (gp-340/DMBT1), a member of the scavenger receptor cysteine-rich superfamily. *J. Biol. Chem.* **277,** 32109–32115
18. Prakobphol, A., Xu, F., Hoang, V. M., Larsson, T., Bergstrom, J., Johansson, I., Frängsmyr, L., Holmskov, U., Leffler, H., Nilsson, C., Borén, T., Wright, J. R., Strömberg, N., and Fisher, S. J. (2000) Salivary agglutinin, which binds *Streptococcus mutans* and *Helicobacter pylori*, is the lung scavenger receptor cysteine-rich protein gp-340. *J. Biol. Chem.* **275,** 39860–39866
19. Oho, T., Yu, H., Yamashita, Y., and Koga, T. (1998) Binding of salivary glycoprotein-secretory immunoglobulin A complex to the surface protein antigen of *Streptococcus mutans*. *Infect. Immun.* **66,** 115–121
20. Demuth, D. R., Lammey, M. S., Huck, M., Lally, E. T., and Malamud, D. (1990) Comparison of *Streptococcus mutans* and *Streptococcus sanguis* receptors for human salivary agglutinin. *Microb. Pathog.* **9,** 199–211
21. Claudianos, C., Dessens, J. T., Trueman, H. E., Arai, M., Mendoza, J., Butcher, G. A., Crompton, T., and Sinden, R. E. (2002) A malaria scavenger receptor-like protein essential for parasite development. *Mol. Microbiol.* **45,** 1473–1484
22. Abrahamsen, M. S., Templeton, T. J., Enomoto, S., Abrahante, J. E., Zhu, G., Lancto, C. A., Deng, M., Liu, C., Widmer, G., Tzipori, S., Buck, G. A., Xu, P., Bankier, A. T., Dear, P. H., Konfortov, B. A., Spriggs, H. F., Iyer, L., Anantharaman, V., Aravind, L., and Kapur, V. (2004) Complete genome sequence of the apicomplexan, *Cryptosporidium parvum*. *Science* **304,** 441–445
23. Hohenester, E., Sasaki, T., and Timpl, R. (1999) Crystal structure of a scavenger receptor cysteine-rich domain sheds light on an ancient superfamily. *Nat. Struct. Biol.* **6,** 228–232
24. Stoddard, E., Cannon, G., Ni, H., Karikó, K., Capodici, J., Malamud, D., and Weissman, D. (2007) gp340 expressed on human genital epithelia binds HIV-1 envelope protein and facilitates viral transmission. *J. Immunol.* **179,** 3126–3132
25. Cummins, J. E., Christensen, L., Lennox, J. L., Bush, T. J., Wu, Z., Malamud, D., Evans-Strickfaden, T., Siddig, A., Caliendo, A. M., Hart, C. E., and Dezzutti, C. S. (2006) Mucosal innate immune factors in the female genital tract are associated with vaginal HIV-1 shedding independent of plasma viral load. *AIDS Res. Hum. Retroviruses* **22,** 788–795
26. Ligtenberg, A. J., Veerman, E. C., Nieuw Amerongen, A. V., and Mollenhauer, J. (2007) Salivary agglutinin/glycoprotein-340/DMBT1: a single molecule with variable composition and with different functions in infection, inflammation and cancer. *Biol. Chem.* **388,** 1275–1289
27. Ligtenberg, A. J., Karlsson, N. G., and Veerman, E. C. (2010) Deleted in malignant brain tumors-1 protein (DMBT1): a pattern recognition receptor with multiple binding sites. *Int. J. Mol. Sci.* **11,** 5212–5233
28. Madsen, J., Mollenhauer, J., and Holmskov, U. (2010) Review: Gp-340/DMBT1 in mucosal innate immunity. *Innate Immun.* **16,** 160–167
29. Malamud, D., Abrams, W. R., Barber, C. A., Weissman, D., Rehtanz, M., and Golub, E. (2011) Antiviral activities in human saliva. *Adv. Dent. Res.* **23,** 34–37
30. Loimaranta, V., Jakubovics, N. S., Hytönen, J., Finne, J., Jenkinson, H. F., and Strömberg, N. (2005) Fluid- or surface-phase human salivary scavenger protein gp340 exposes different bacterial recognition properties. *Infect. Immun.* **73,** 2245–2252
31. Bikker, F. J., Ligtenberg, A. J., End, C., Renner, M., Blaich, S., Lyer, S., Wittig, R., van't Hof, W., Veerman, E. C., Nazmi, K., de Blieck-Hogervorst, J. M., Kioschis, P., Nieuw Amerongen, A. V., Poustka, A., and Mollenhauer, J. (2004) Bacteria binding by DMBT1/SAG/gp-340 is confined to the VEVL*XXXX*W motif in its scavenger receptor cysteine-rich domains. *J. Biol. Chem.* **279,** 47699–47703
32. Jakubovics, N. S., Strömberg, N., van Dolleweerd, C. J., Kelly, C. G., and Jenkinson, H. F. (2005) Differential binding specificities of oral streptococcal antigen I/II family adhesins for human or bacterial ligands. *Mol. Microbiol.* **55,** 1591–1605
33. Purushotham, S., and Deivanayagam, C. (2013) Cloning, expression and purification of the SRCR domains of glycoprotein 340. *Protein Expr. Purif.* **90,** 67–73
34. Brady, L. J., Piacentini, D. A., Crowley, P. J., Oyston, P. C., and Bleiweis, A. S. (1992) Differentiation of salivary agglutinin-mediated adherence and aggregation of mutans streptococci by use of monoclonal antibodies against the major surface adhesin P1. *Infect. Immun.* **60,** 1008–1017
35. Oli, M. W., McArthur, W. P., and Brady, L. J. (2006) A whole cell BIAcore assay to evaluate P1-mediated adherence of *Streptococcus mutans* to human salivary agglutinin and inhibition by specific antibodies. *J. Microbiol. Methods* **65,** 503–511

36. Schuck, P. (1997) Use of surface plasmon resonance to probe the equilibrium and dynamic aspects of interactions between biological macromolecules. *Annu. Rev. Biophys. Biomol. Struct.* **26,** 541–566
37. Hobb, R. I., Tzeng, Y. L., Choudhury, B. P., Carlson, R. W., and Stephens, D. S. (2010) Requirement of NMB0065 for connecting assembly and export of sialic acid capsular polysaccharides in *Neisseria meningitidis*. *Microbes Infect.* **12,** 476–487
38. Sreerama, N., and Woody, R. W. (2000) Estimation of protein secondary structure from circular dichroism spectra: comparison of CONTIN, SELCON, and CDSSTR methods with an expanded reference set. *Anal. Biochem.* **287,** 252–260
39. Yang, Z. R., Tendian, S. W., Carson, W. M., Brouillette, W. J., Delucas, L. J., and Brouillette, C. G. (2004) Dimethyl sulfoxide at 2.5% (v/v) alters the structural cooperativity and unfolding mechanism of dimeric bacterial NAD^+ synthetase. *Protein Sci.* **13,** 830–841
40. Lebowitz, J., Lewis, M. S., and Schuck, P. (2002) Modern analytical ultracentrifugation in protein science: a tutorial review. *Protein Sci.* **11,** 2067–2079
41. Schuck, P. (2000) Size-distribution analysis of macromolecules by sedimentation velocity ultracentrifugation and lamm equation modeling. *Biophys. J.* **78,** 1606–1619
42. Rodamilans, B., Muñoz, I. G., Bragado-Nilsson, E., Sarrias, M. R., Padilla, O., Blanco, F. J., Lozano, F., and Montoya, G. (2007) Crystal structure of the third extracellular domain of CD5 reveals the fold of a group B scavenger cysteine-rich receptor domain. *J. Biol. Chem.* **282,** 12669–12677
43. Ojala, J. R., Pikkarainen, T., Tuuttila, A., Sandalova, T., and Tryggvason, K. (2007) Crystal structure of the cysteine-rich domain of scavenger receptor MARCO reveals the presence of a basic and an acidic cluster that both contribute to ligand recognition. *J. Biol. Chem.* **282,** 16654–16666
44. Somoza, J. R., Ho, J. D., Luong, C., Ghate, M., Sprengeler, P. A., Mortara, K., Shrader, W. D., Sperandio, D., Chan, H., McGrath, M. E., and Katz, B. A. (2003) The structure of the extracellular region of human hepsin reveals a serine protease domain and a novel scavenger receptor cysteine-rich (SRCR) domain. *Structure* **11,** 1123–1131
45. Lamont, R. J., Demuth, D. R., Davis, C. A., Malamud, D., and Rosan, B. (1991) Salivary-agglutinin-mediated adherence of Streptococcus mutans to early plaque bacteria. *Infect. Immun.* **59,** 3446–3450
46. Esberg, A., Löfgren-Burström, A., Ohman, U., and Strömberg, N. (2012) Host and bacterial phenotype variation in adhesion of *Streptococcus mutans* to matched human hosts. *Infect. Immun.* **80,** 3869–3879
47. Ligtenberg, T. J., Bikker, F. J., Groenink, J., Tornoe, I., Leth-Larsen, R., Veerman, E. C., Nieuw Amerongen, A. V., and Holmskov, U. (2001) Human salivary agglutinin binds to lung surfactant protein-D and is identical with scavenger receptor protein gp-340. *Biochem. J.* **359,** 243–248
48. Christopeit, T., Gossas, T., and Danielson, U. H. (2009) Characterization of Ca^{2+} and phosphocholine interactions with C-reactive protein using a surface plasmon resonance biosensor. *Anal. Biochem.* **391,** 39–44
49. Young, A., Rykke, M., Smistad, G., and Rølla, G. (1997) On the role of human salivary micelle-like globules in bacterial agglutination. *Eur. J. Oral Sci.* **105,** 485–494
50. Jovine, L., Darie, C. C., Litscher, E. S., and Wassarman, P. M. (2005) Zona pellucida domain proteins. *Annu. Rev. Biochem.* **74,** 83–114
51. Wu, Z., Lee, S., Abrams, W., Weissman, D., and Malamud, D. (2006) The N-terminal SRCR-SID domain of gp-340 interacts with HIV type 1 gp120 sequences and inhibits viral infection. *AIDS Res. Hum. Retroviruses* **22,** 508–515
52. Stoddard, E., Ni, H., Cannon, G., Zhou, C., Kallenbach, N., Malamud, D., and Weissman, D. (2009) gp340 promotes transcytosis of human immunodeficiency virus type 1 in genital tract-derived cell lines and primary endocervical tissue. *J. Virol.* **83,** 8596–8603